LBL-30022

Lawrence Berkeley Laboratory
UNIVERSITY OF CALIFORNIA

Presented at the Committee on Space Research
XXVII Plenary Meeting, The Hague, The
Netherlands, June 25–July 6, 1990, and
to be published in the Proceedings

Ground-Based Measurements of Galactic Cosmic Ray Fragmentation in Shielding

W. Schimmerling

November 1990

Donner Laboratory

Biology & Medicine Division

LOAN COPY
Circulates
for 4 weeks
Bldg. 50 Library.
LBL-30022
Copy 2

Prepared for the U.S. Department of Energy under Contract Number DE-AC03-76SF00098.

DISCLAIMER

This document was prepared as an account of work sponsored by the United States Government. While this document is believed to contain correct information, neither the United States Government nor any agency thereof, nor the Regents of the University of California, nor any of their employees, makes any warranty, express or implied, or assumes any legal responsibility for the accuracy, completeness, or usefulness of any information, apparatus, product, or process disclosed, or represents that its use would not infringe privately owned rights. Reference herein to any specific commercial product, process, or service by its trade name, trademark, manufacturer, or otherwise, does not necessarily constitute or imply its endorsement, recommendation, or favoring by the United States Government or any agency thereof, or the Regents of the University of California. The views and opinions of authors expressed herein do not necessarily state or reflect those of the United States Government or any agency thereof or the Regents of the University of California.

GROUND-BASED MEASUREMENTS OF GALACTIC COSMIC RAY FRAGMENTATION IN SHIELDING*,**

Walter Schimmerling

Lawrence Berkeley Laboratory, Berkeley, CA 94720 and Jet Propulsion Laboratory, Pasadena, CA 91109.

ABSTRACT

The mean free path for nuclear interactions of galactic cosmic rays is comparable to shielding and tissue thicknesses present in human interplanetary exploration, resulting in a significant fraction of nuclear reaction products at depth. In order to characterize the radiation field, the energy spectrum, the angular distribution, and the multiplicity of each type of secondary particles must also be known as a function of depth. Reactions can take place anywhere in a thick absorber; therefore, it is necessary to know these quantities as a function of particle energy for all particles produced. HZE transport methods are used to predict the radiation field; they are dependent on models of the interaction of man–made systems with the space environment to an even greater extent than methods used for other types of radiation. Hence, there is a major need to validate these transport codes by comparison with experimental data. The most cost-effective method of validation is a comparison with ground-based experimental measurements. A research program to provide such validation measurements using neon, iron and other accelerated heavy ion beams will be discussed and illustrated using results from ongoing experiments and their comparison with current transport codes. The extent to which physical measurements yield radiobiological predictions will be discussed.

INTRODUCTION

The radiation field of relativistic heavy ions at depth is altered by nuclear reactions of the incident particles with the matter present in spacecraft shielding materials and furnishings and in traversed tissue. In these reactions, particles of different charge and mass are emitted with different angular distributions /1,2/ and each nuclear interaction event can have an associated multiplicity of more than one emerging interaction product. The presence of these nuclear reaction products has a significant impact upon the radiation quality /3,4/. This impact increases with depth of penetration; in particular, the exit dose of high–energy heavy charged–particle beams used in radiotherapy is entirely due to fragments emitted from nuclear interactions of the primary beam.

The probabilities for nuclear interactions are generally determined in materials thin compared with the range and the nuclear mean free path of the traversing charged particles, so that energy loss and multiple nuclear collisions can be neglected. In bulk matter, on the other hand, energy loss of incident and emitted particles cannot be neglected, so that the dependence of the cross sections on the projectile energy must be considered. Multiple interactions also become more probable

*Supported in part by the Public Health Service of the U.S. Department of Health and Human Services under Grant No. CA23247 awarded by the National Cancer Institute and in part by the National Aeronautics and Space Administration and conducted at the Lawrence Berkeley Laboratory (Department of Energy contract DE-AC03-76SF00098 to the University of California).

**The work of the author was carried out in collaboration with M. Shavers, J. Miller, L. Townsend, J. Wilson, S. Curtis, E. Lampo, R. Leres, D. Landis, J. Walton, H. Spieler, M. Wong, M. Rapkin, and M. Phillips.

in thick absorbers. Multiple Coulomb scattering will result in a distribution of incident and emitted particle directions and nuclear reactions of previously emitted nuclear reaction products will change the yields of particles at depth from what is predicted based on simple cross section calculations. This type of interaction of radiation with bulk matter is usually addressed by the use of *transport calculations.*

A radiation transport calculation is, in effect, the solution of a three-dimensional diffusion equation. The solution can be obtained analytically or by means of Monte Carlo simulation methods. In either case, what is required is an accurate knowledge of nuclear cross sections and of the energy loss of all particles present at any depth of material. Cross sections are needed for the production of all possible particles in all possible final states, for the interaction of the primary incident nuclei with matter, and for subsequent interactions of previously emitted reaction products. The required cross sections will, in general, be differential in energy, in angle and in particle multiplicity. At the present time, measurements of most of the cross sections of interest do not exist; their understanding is part of the developing field of heavy ion physics and reliable methods for their prediction in general are not available. Silberberg and Tsao /5/ have developed semi-empirical formulae to interpolate between results of a systematic compilation of (integral) fragmentation cross sections, and methods for estimating nuclear cross sections for space radiation transport calculations are being developed by Townsend and Wilson /6/.

There is a clear need for a more extensive data base of differential fragmentation cross sections to be used as input to and for validation of transport calculations, but the infeasibility of obtaining systematic data from cosmic rays alone makes ground-based measurements necessary. Consequently, we have undertaken a program to make a series of measurements of heavy ion fragmentation cross sections at the Lawrence Berkeley Laboratory Bevalac. Data for 670 MeV/nucleon (MeV/u) ^{20}Ne incident on a variable thickness water column have recently been published /7/, and comparison of these data with the results of an analytical calculation using the HZESEC computer code (see below) revealed agreement at the 30% level between measured and calculated integrated fluences of fragments for thin water absorbers. Agreement between calculation and experiment was not as good for the distributions of fluence as a function of linear energy transfer (LET) in water ("fluence spectra"), reflecting the extreme sensitivity of such calculations to the accuracy of the energy loss calculations in the stopping region. The effect of the approximations inherent in the calculation and the constraints placed on experiment in this type of work were also studied /8/. In this paper, the experimental distributions of fluence are compared with the predictions of an additional analytical computer code, LBLBEAM, in order to better understand some of these problems.

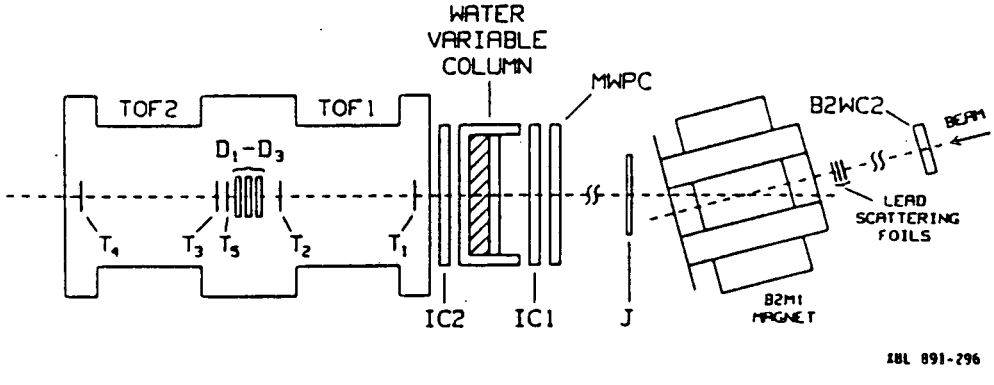

Fig. 1. Schematic of the beamline and detectors.

EXPERIMENTAL APPARATUS AND METHODS

The experimental data were obtained from a series of experiments conducted at the Bevalac in the beam line depicted schematically in Fig. 1. The apparatus and methods are described in detail

in /7/. The design describes beam interactions by particle identification and direct measurements of fluence and velocity.

The beam passed through scintillation counter J used for beam monitoring and normalization, a multiwire proportional counter (MWPC) that monitors beam profile, the first of two ionization chambers, IC_0, a variable depth water column, and the second ionization chamber, IC_1. The Bragg curve is obtained from the ratio of measured ionizations IC_1/IC_0, normalized to the zero water position of the water column.

The fragment identification apparatus consists of dual time-of-flight (TOF) telescopes, $T_1 - T_2$ and $T_3 - T_4$, between which are placed finite energy loss (ΔE) silicon detectors $D_1 - D_3$. Folding together time of flight and energy loss allowed us to separate fragments according to their charge and atomic mass; the precise analysis procedure varied somewhat according to the water column thickness. Figure 2 shows a scatterplot of energy loss in detector $D1$ vs. fragment velocity (obtained from the time of flight) for neon ions incident on 25 cm of water. Bands corresponding to different fragments are clearly visible. Nuclei from Be (Z=4) through Ne (Z=10) were identified in this way; lighter nuclei did not deposit sufficient energy in the detectors to register above the detector threshold. For small absorber thicknesses, this was also true for Z=4 (and, in some cases, for Z=5), resulting in an efficiency loss of undetermined magnitude.

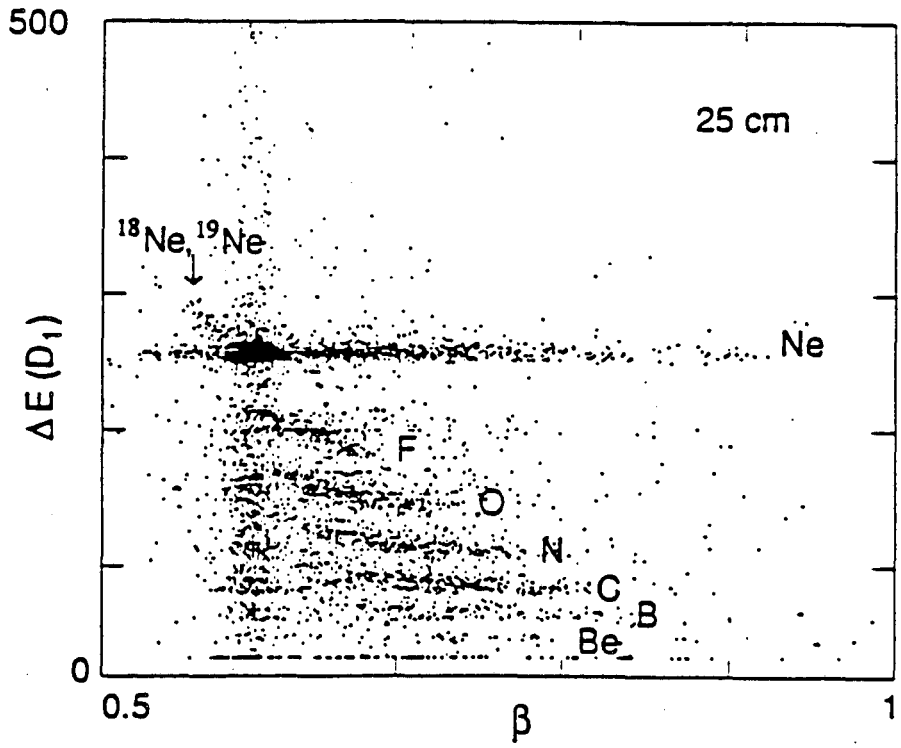

XBL 893-746

Fig. 2. Scatterplot of energy loss vs. fragment velocity for fragments produced by neon projectiles incident on 25 cm of water.

The LET_∞ (abbreviated below as LET) of each particle was calculated using the particle velocity and charge. The fluence spectra for each fregment were obtained for each water thickness; integration over these spectra yielded the integral number of fragments of each species, also as a

function of water thickness.

TRANSPORT CALCULATIONS

HZESEC

HZESEC is a transport code written to calculate various distributions of physical parameters of interest at arbitrary depths in water and other materials for narrow energy-width stopping heavy ion beams. It was developed by Curtis /9/ and modified by Schimmerling *et al.* /10/.

HZESEC assumes that the straight ahead approximation is valid; *i.e.*, the nuclear interaction products proceed in the same direction as the primaries and continue with the energy that the primary had at the point of interaction. The point of interaction is determined by assuming that all fragments are the results of an interaction of the primary beam with the material, *i.e.*, higher order reaction products are neglected. The error introduced by this approximation will be greatest for the fragments of the lightest elements, corresponding to mass M_k, which can be produced by all particles of mass M_j intermediate between M_k and the mass of the primary beam. Primary and secondary particles are attenuated as an exponential function of constant nuclear mean free path, λ. For each element of charge $Z < Z_{primary}$, only one isotopic mass is assumed, corresponding to that mass with the highest production cross section /9/. A separate calculation of the acceptance is used to account for the effects of detector geometry and multiple scattering /11/. The calculation accounts for spreading of the beam range and energy due to the initial energy distribution of a heavy ion beam.

The assumption that all fragments are produced by the primary incident beam *i.e.*, that secondary particles do not interact to produce tertiaries and higher order generations of fragments, makes it possible to determine the interaction depth at which a secondary with a given LET was produced. This follows from using the range-energy relation for projectile and fragment to ascertain the point at which both particles had the same velocity. Consequently, for every thickness x of the water absorber, the LET spectra of these first generation secondaries have an upper and lower limit. The upper limit of high LET corresponds to the secondary particle with the lowest velocity. Since energy loss in the absorber is a function of Z^2, the lowest velocity will be obtained when energy is lost by the primary throughout the absorber and the lighter secondary is produced at the exit face. Conversely, the lower limit of LET, corresponding to the maximum velocity secondary particle, will be obtained when energy loss in the absorber can be ascribed to the secondary particle throughout the absorber thickness, *i.e.*, when the secondary has been produced at the entrance of the absorber.

Stopping power is determined for protons according to the technique of Bichsel /12/ which uses a piece-wise fit to power functions of energy over short energy intervals. The stopping power, $S_j(E_j)$, of a heavy ion Z_j with a total kinetic energy E_j, is obtained by scaling the stopping power S of protons according to

$$S_j(E_j) = Z_j^2 S(\epsilon). \tag{1}$$

where ϵ is the equivalent proton energy.

The microscopic nuclear cross sections $\sigma_{abs}(i,j)$ are obtained from an energy-independent form of the Bradt-Peters parameterization /14/:

$$\sigma_{abs}(i,j) = 10 \times \pi \times r_0^2 \times (A_i^{1/3} + A_j^{1/3} - C)^2 \tag{2}$$

where $r_0 = 1.29$ fm, $A_k (k = i, j)$ are the mass numbers of the colliding nuclei, and $C = 1 - 0.028 \times$ the lowest of the two mass numbers. The number of fragments of a given type produced per interaction, or multiplicity, is given by the ratio of the fragmentation cross section to the reaction cross section. The fragmentation cross sections are obtained from the semi-empirical formulae of Silberberg and Tsao /5/ for proton-nucleus collisions. In order to separate the velocity dependence of these cross sections from their absolute values, the cross sections are normalized to their values at $2.1A$ GeV ($\beta = 0.95$) and tabulated as a function of velocity for subsequent use in the calculation /10/. The Silberberg and Tsao formulae do not provide values for fragments lighter than ^{6}He; an extension to light product nuclei, proposed by Letaw /13/ has not yet been included.

The accuracy of these formulae has been examined /14/ and found to be of the order of 30% for the reactions examined. For reactions and projectile energies that are not a part of the data set for which Silberberg and Tsao provide interpolations, substantially greater discrepancies may exist and cannot be estimated beforehand.

LBLBEAM

The heavy-ion transport code LBLBEAM was developed at NASA-Langley Research Center. The key approach was to use a perturbative solution of a one-dimensional Boltzmann transport equation. The transport problem is in steady state with a boundary condition at the entrance to the absorber. The Boltzmann transport equation in the straight-ahead-approximation and neglecting target secondary fragments is written as

$$\left[\frac{\partial}{\partial x} - \tilde{S}_j(E)\frac{\partial}{\partial E} + \sigma_j(E)\right]\phi_j(x,E) = \sum_{k>j}\sigma_{jk}(E,E')m_{jk}(E)\phi_k(x,E') \tag{3}$$

with the boundary condition

$$\phi_j(0,E) = \delta_{ij}\frac{1}{\sqrt{2\pi}\sigma}e^{-\frac{(E-E_0)^2}{2\sigma^2}}. \tag{4}$$

Using perturbation theory, the analytic solution of the problem is given by

$$\begin{aligned}\phi(x,E) = & \\ & \frac{\{S_j(E)P_j(E)\phi_j(x,E)\}_{bdry}}{S_j(E)P_j(E)} \\ & + \sum_k \int_E^{E_{bdry}} dE' \frac{A_j P_j(E')}{S_j(E)P_j(E)} m_{jk}(E')\sigma_k(E') \cdot \phi_k\{x + R_j(E) - R_j(E'), E'\} \\ = & \ \phi_j^{(primary)} + \phi_j^{(secondaries)} + \phi_j^{(tertiaries)} + \ldots\ldots\end{aligned} \tag{5}$$

The flux of ions $\phi_j(x,E)$ of type j with atomic mass A_j at x move along the x-axis at energy E, in units of MeV/u. $\sigma_j(E)$ is the corresponding nuclear absorption cross section for the jth ion interacting in water. $m_{jk}(E)\sigma_k(E)$ is the production cross section for type j ions by collision of type k ions with a target nucleus.

The transport equation is solved by the method of characteristics using an iterative procedure. The primary term $\phi_j^{(primary)}$ is obtained by following the attenuated and degraded beam incident on the absorber boundary. The secondary term is obtained by substituting the primary term into the integral expression. Similarly, the tertiary term is obtained by substituting the secondary term into the integral expression. Higher order terms can be obtained by following this iterative procedure /15/.

Interaction Parameters

The LBLBEAM code uses an elaborate scheme to calculate stopping power, that is coded in a modular form. For this reason, it proved convenient to change the stopping power calculation used and introduce into the computer program the same method used to obtain experimental LET values from the measured time of flight and charge of the particles /11/, which had been found to reproduce well their energy loss throughout the absorber thicknesses used. In this way, it was possible to obtain a stopping-power independent calculation.

The nuclear fragmentation parameters are the same as those used by the HZESEC model /5/. The fragmentation parameters are evaluated at the total kinetic energy (rather than energy per nucleon) of the target atom as seen in the projectile rest frame. The target fragments resulting from central collisions are not included since they are assumed to be produced at large angles

and do not contribute in the forward direction. The production cross sections are averaged over the shield material constituents.

COMPARISON OF MODELS WITH DATA

A detailed comparison between the neon fluence spectra and the theory is shown in Figs. 3 and 4. The ordinate units are given in fluence per LET interval (keV/μm), per unit incident beam fluence. The vertical scales are different from panel to panel in order to accomodate the changing numbers of particles with depth. The abcissa in every panel, in units of keV/μm, also changes scale from panel to panel in order to present the full spectrum of particles. The theoretical prediction of each model, multiplied by the calculated acceptance of the detector at each value of LET, is the predicted fluence, $\phi_{th}(x, Z; L_i)$, which has been plotted as the histogram in the figures; the measured data have been plotted as the filled circles. Where error bars are not visible, they are smaller than the size of the plotting symbol; errors shown are statistical and not systematic. Details of the methods used are given in /8/.

For neon in the plateau region of the Bragg curve, agreement between data and LBLBEAM is good down to the level where fluence is 1% of its maximum value. Differences between data and model in the high LET tail region can be attributed to neon isotopes, which are not explicitly taken into account in the theory. For water thicknesses greater than 25 g/cm^2 the difference between HZESEC and the data can be attributed almost entirely to the range energy calculation employed by HZESEC, which leads to a prediction of significantly lower fluences. The nuclear mean free path from the experimental data, $\lambda_{exp} = 16.5$ g/cm^2; from LBLBEAM, $\lambda_{LBL} = 16.0$ g/cm^2; from HZESEC, $\lambda_{HZE} = 15.4$ g/cm^2.

The HZESEC model calculates projectile fragments resulting from the nuclear fragmentation of the incident neon only, without taking into consideration secondary or higher order interactions. In Fig. 5 the differential fluence spectra $\phi(x, Z = 6; L)$ for carbon calculated by HZESEC are compared with the data for the full range of water thicknesses. For water thicknesses up to 20 g/cm^2 the predicted fluences overlap with experimental data within the 30% accuracy attributed to the cross sections. Discrepancies appear mainly in the high LET tail.

Figure 6 illustrates the LBLBEAM predictions for first generation carbon. In this case, detector geometry was taken into consideration separately for each isotope, and the stopping power calculation is the same as used for the experimental data. The fluences predicted by LBLBEAM for carbon are within 30% at water thicknesses up to approximately 30 g/cm^2.

For increasing absorber thickness and decreasing fragment mass, the number of possible reaction channels increases and higher order interactions become more likely. Figure 7 illustrates the effect of including *tertiary* fragments in the LBLBEAM calculation of carbon fluence spectra. Although this is not clearly visible on the semilogarithmic scale of the plots, approximately 33% of the fluence predicted by LBLBEAM for water absorber thicker than 30 cm is due to tertiary interactions *i.e.*, carbon produced in two successive nuclear interactions.

Greater insight into the implications of the comparison can be obtained from Fig. 8, which compares the total number of particles of each detected element (integral fluences) as a function of water thickness over the entire range covered by the experiment. The full circles denote the experimental data as before; the full-line histogram is the prediction of HZESEC, the dashed-line histogram is the prediction of LBLBEAM based on one-generation secondaries only, and the dotted-line histogram is the prediction of LBLBEAM including tertiaries from two generations of nuclear interactions.

The threshold effect of the detector can be seen in the panels for the Be and B data, where the measured number of Be fragments falls significantly below all predictions for absorber thicknesses less than 25 g/cm^2; B seems to deposit signals above threshold at thicknesses greater than approximately 15 g/cm^2.

The predictions of HZESEC are systematically lower than those of LBLBEAM, even for the lighter fragments, where differences in stopping power calculations are not significant. One way in which such behavior could arise is if one of the models did not properly account for the lower mass

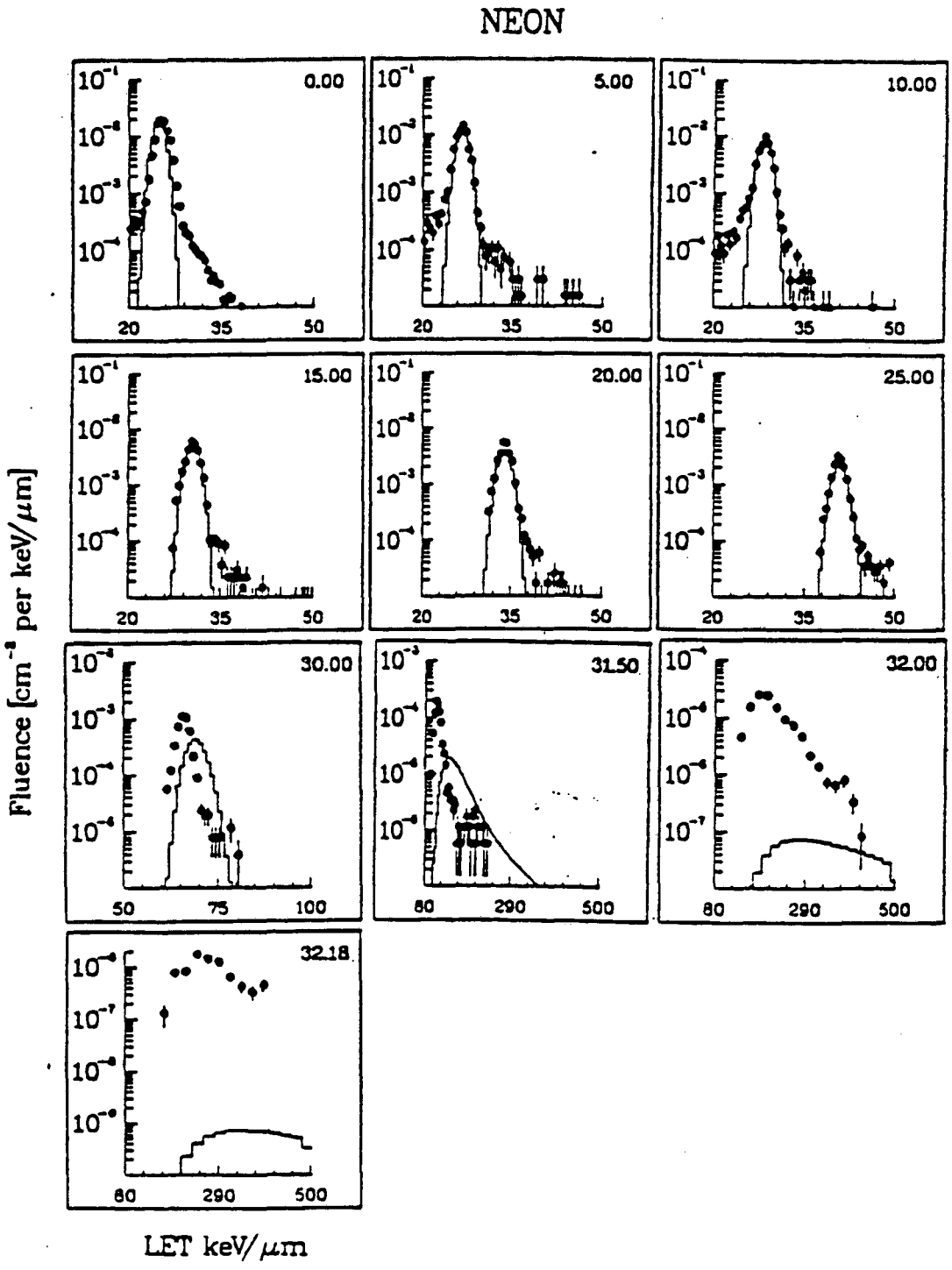

Fig. 3. Differential fluence for neon nuclei incident on various thicknesses of water (shown at the upper right of each panel in gm/cm^2). The solid circles represent the data; the histogram shows the results of the HZESEC calculation. (From Ref. /8/.)

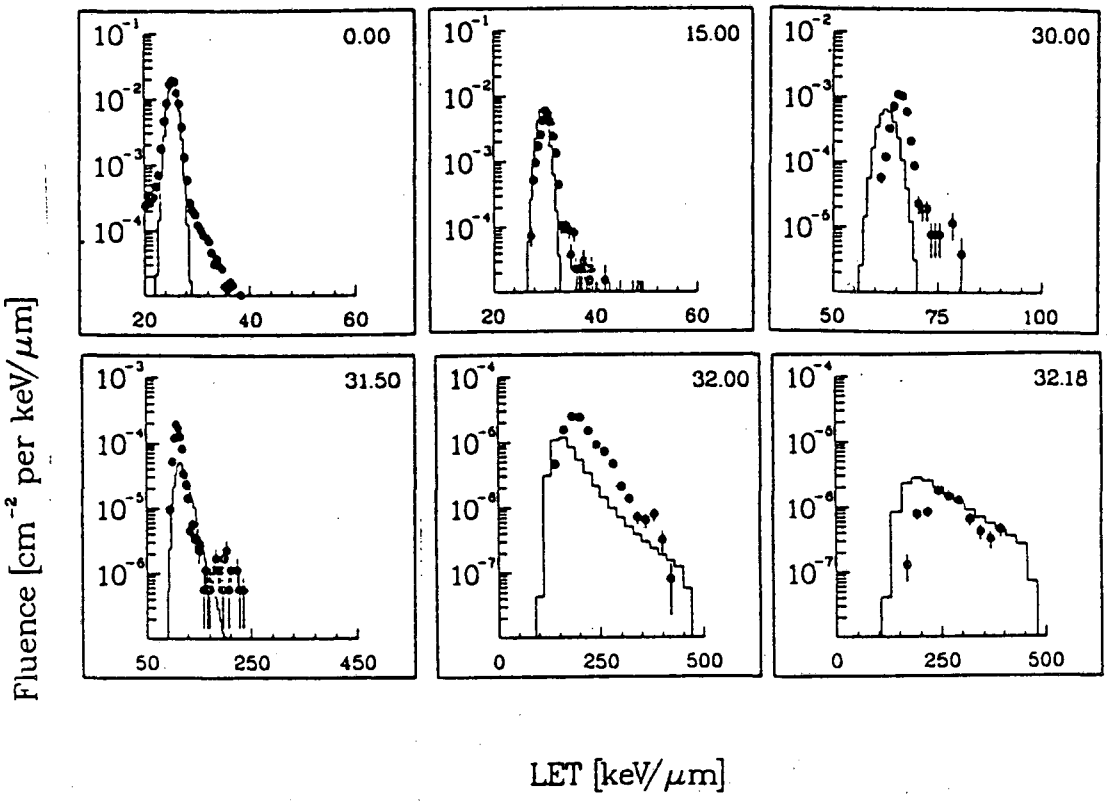

Fig. 4. Differential fluence for neon nuclei incident on various thicknesses of water. The solid circles represent the data; the histogram shows the results of the LBLBEAM calculation.

isotopes. Such an effect may be a consequence of the fact that the fragmentation cross sections used by LBLBEAM, obtained from the latest semi-empirical fits of Silberberg and Tsao, are larger than the older values employed by HZESEC.

The difference between the one-generation and the two-generation predictions of LBLBEAM show the expected effect of tertiaries, which increases for lighter particles and thicker absorber; however, the tertiary prediction of LBLBEAM is systematically greater than the data. One likely reason for this behavior must lie with the angular distribution of the fragments, which is not taken into account in the straight-ahead approximation used by the transport code. Two effects contribute to the angular distribution of fragments. One of these effects is the compounding of the angular distributions of fragments emitted in nuclear interactions, which results in fewer fragments emitted into the narrow solid angle of the detector. The other effect is that the velocity of tertiary particles emerging from the absorber is no longer uniquely tied to the position at which it is produced and, therefore the scattering calculation used for the acceptance will be based on an erroneous amount of scattering material.

It is not immediately apparent that the more recent values of the cross sections are more accurate than the older values. The one-generation predictions of LBLBEAM may also be too large, if the geometric effects discussed above do not result in significant differences between predicted secondaries and tertiaries. If this is the case, then the predictions of LBLBEAM would be expected to be below the measured data by an amount equivalent to the added contribution of tertiaries, which is approximately the difference seen by HZESEC.

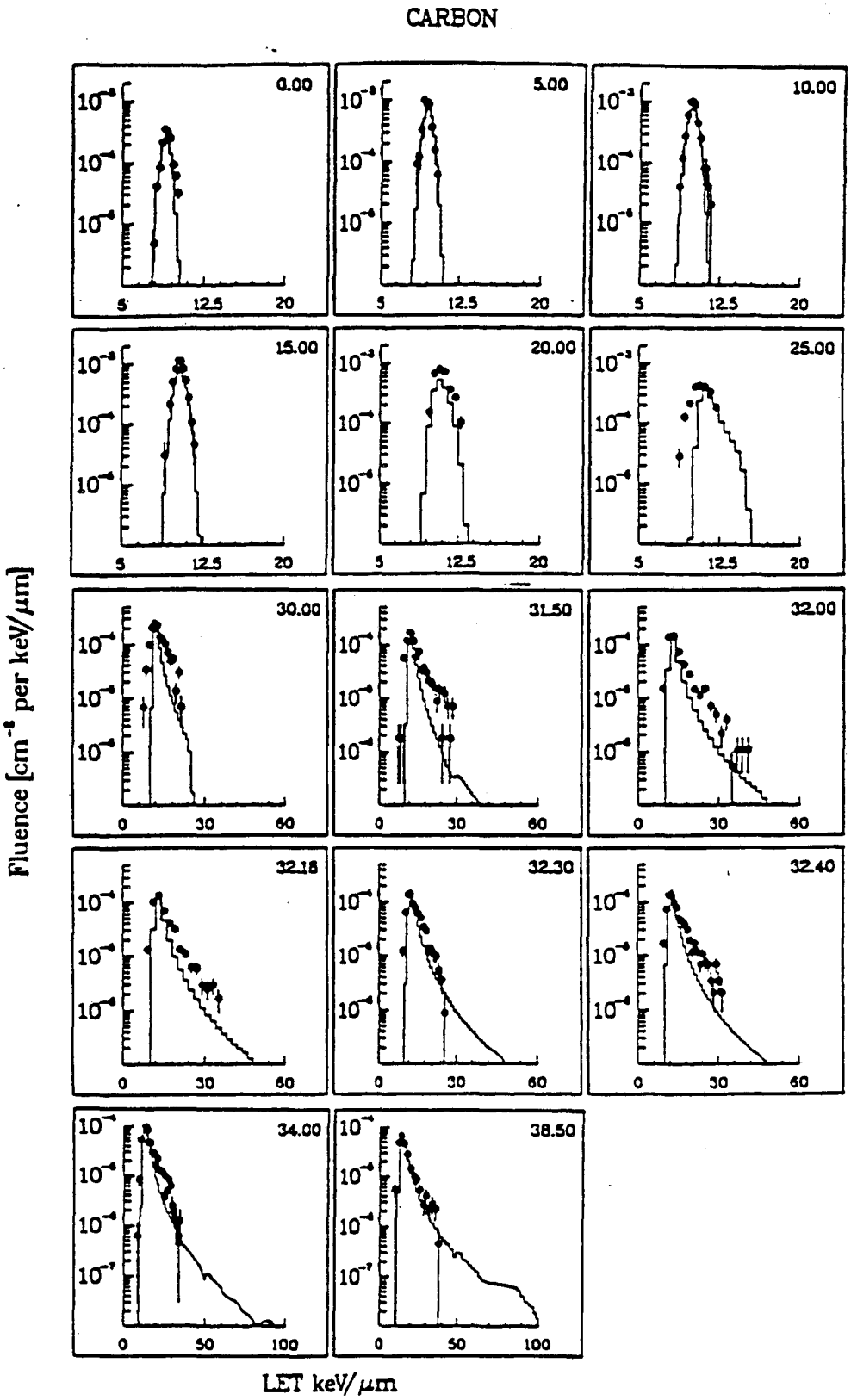

Fig. 5. Differential fluence for carbon nuclei produced by neon nuclei incident on various thicknesses of water. The solid circles represent the data; the histogram shows the results of the HZESEC calculation. (From Ref. /8/.)

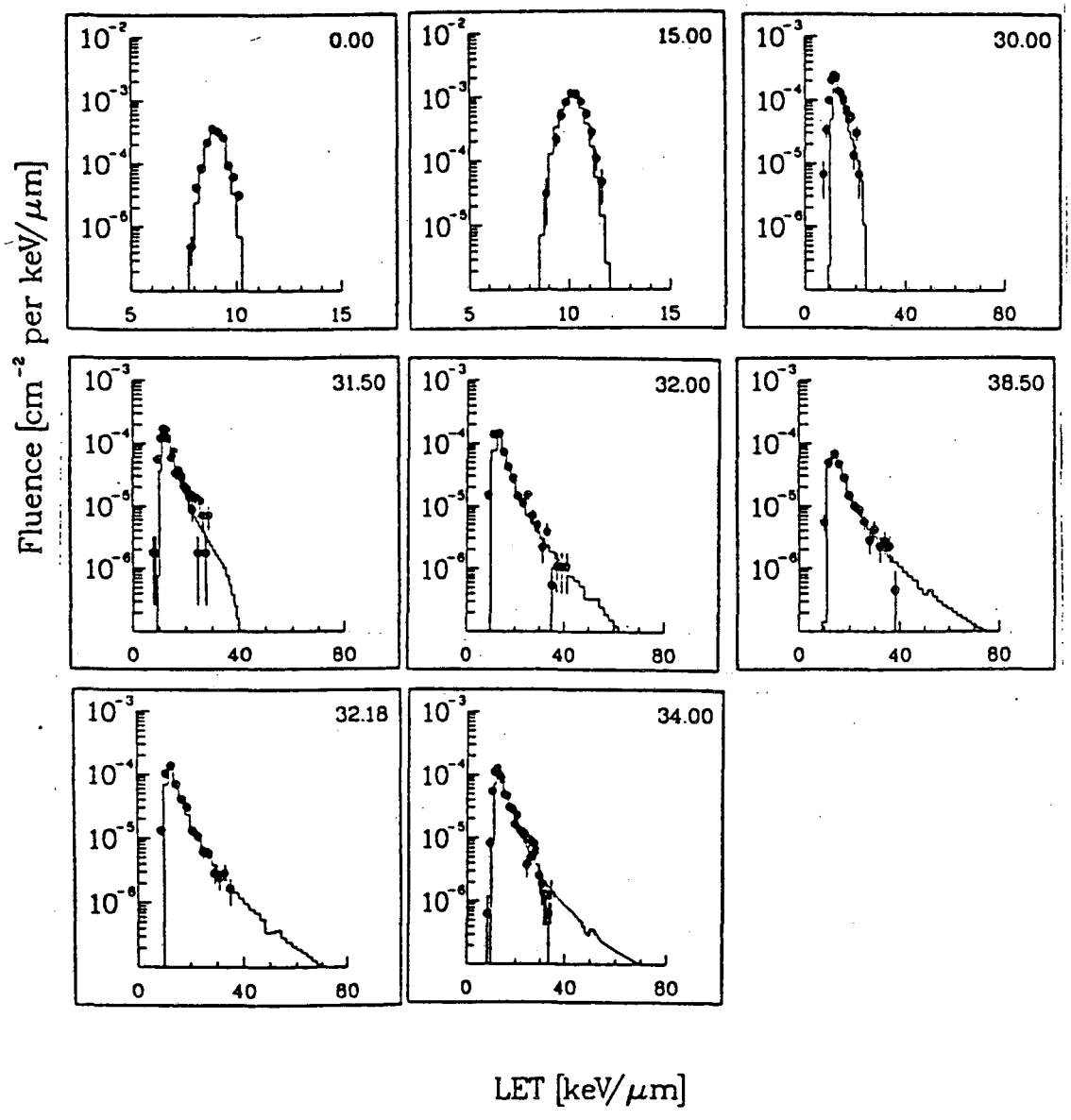

Fig. 6. Differential fluence for carbon nuclei produced by neon nuclei incident on various thicknesses of water. The solid circles represent the data; the histogram shows the results of the LBLBEAM calculation.

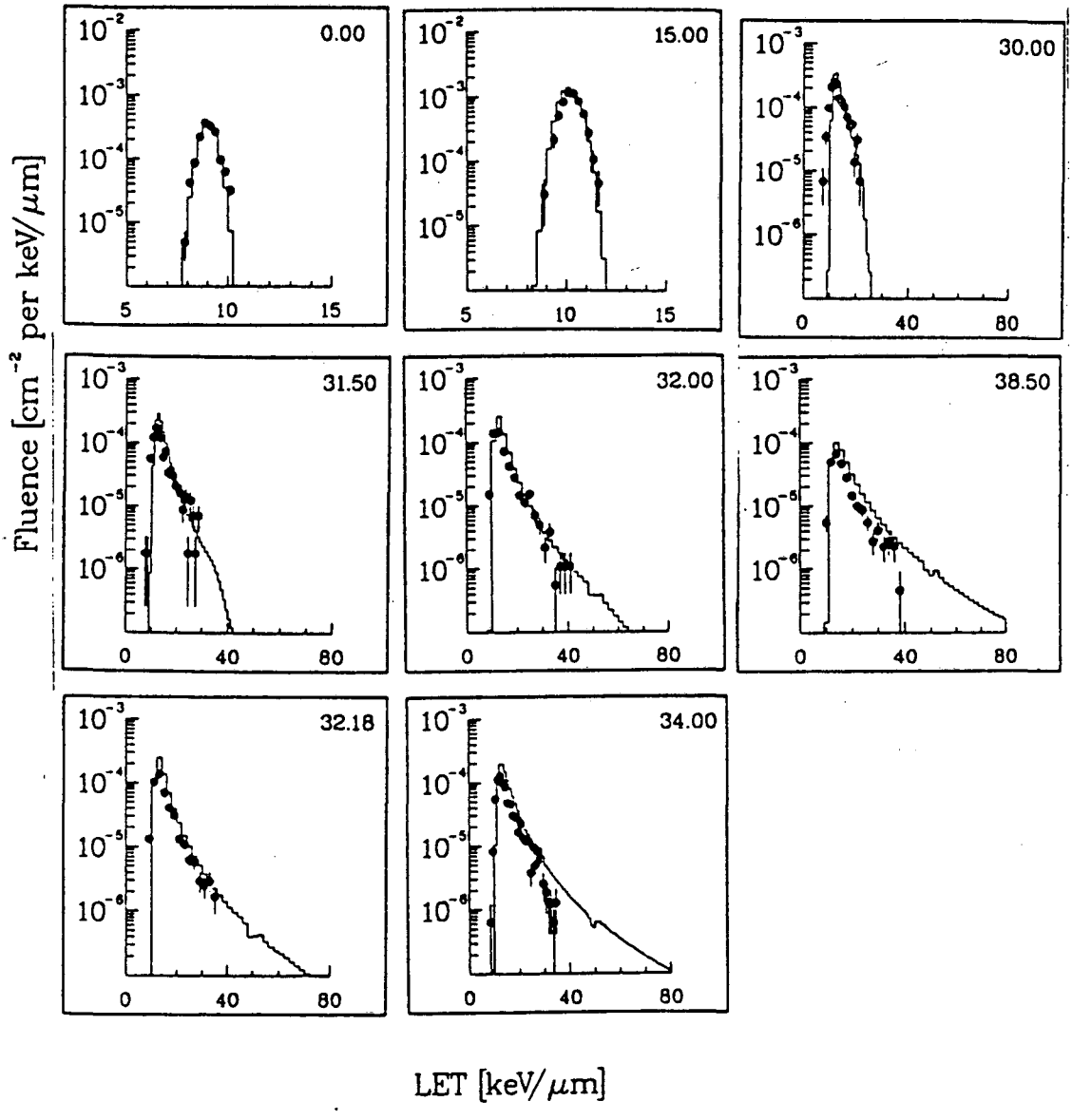

Fig. 7. Differential fluence for carbon nuclei produced by neon nuclei incident on various thicknesses of water. The solid circles represent the data; the histogram shows the results of the LBLBEAM calculation, with tertiary fragments included.

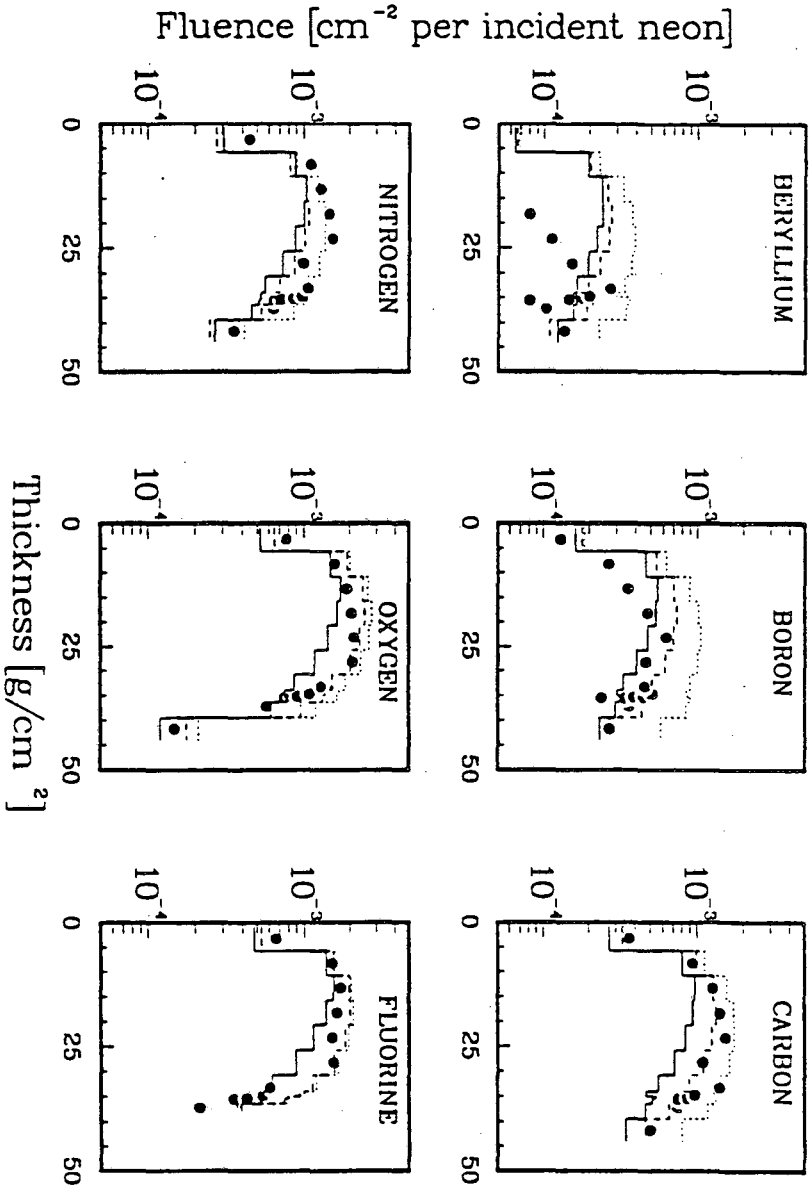

Fig. 8. Integral fluence for all fragments produced by neon nuclei incident on various thicknesses of water, as a function of water column thickness. Full circles: experiment, full lines: HZESEC, broken lines: LBLBEAM (one generation fragments), dotted lines: LBLBEAM (two-generation fragments).

BIOLOGICAL INTERPRETATIONS

If the relative biological effectiveness (RBE) is known for each particle at every value of LET, then an average, $\overline{RBE}$, can be calculated /4/ for the radiation field at depth:

$$\overline{RBE(x)} = \sum_Z \int_0^{L_{max}} R(L)\phi(x,Z,L)LdL / \sum_Z \int_0^{L_{max}} \phi(x,Z,L)LdL, \qquad (6)$$

where R(L) is RBE assumed to be a function only of LET. The results, for the case of spermatogonial cell survival obtained from testes weight loss /4/, are shown in Fig. 9. The full circles are values calculated using Eq. 6, with R(L) fitted to measurements of spermatogonial cell survival in monoenergetic beams with negligible fragmentation components. The open circles are actual measurements of RBE, using the same testes weight loss model, this time in the mixed radiation field at the four absorber thicknesses. The Bragg curve (dotted line) is shown to place the thicknesses in the context of the primary particle range.

As shown in Fig. 9, the calculated RBE at 0 cm, where the neon beam less than approximately 6%, agrees within 5% with the measured value, indicating the level of biological reproducibility that can be achieved with this model system. The other biological results differ from the calculated value by approximately 10% at 20 and 30 cm, and by almost 40% at 33 cm of water. The observed difference between RBE predicted from fluence spectra and the measured RBE is attributed to two factors. At 20 and 30 cm, the discrepancy is attributed mainly to the fact that, in the corresponding region of LET, the fit to RBE used in the calculation has a large contribution from plateau silicon, whereas the mixed-field RBE is dominated by residual neon. The pattern of energy deposition of the particles used to calculate RBE is significantly different from that of the particles used in the measurement, illustrating the type of effect expected from track structure differences.

In the stopping region of the neon beam, the discrepancy between measured and calculated RBE is also attributable to the fact that the experiment does not detect lighter particles with $Z \leq 3$. In order to account for the observed reduction in RBE, lighter particles would have to contribute almost 80% of the total dose at this depth. The extent to which this is true was not ascertained in this experiment.

Other methods to interpret fluence spectra have been developed /16/, and these methods will no doubt become prevalent as predictions of biological effects of high energy, highly charged (HZE) particles, such as are found in galactic cosmic rays, become critical for human space exploration.

CONCLUSIONS

Physical measurements of fluence spectra, whereby the products of the nuclear interactions of incident energetic heavy ions are identified and measured directly, are a powerful method to understand the radiation field at depth in tissue-equivalent and shielding materials. They provide a detailed test of transport methods and allow a determination of those aspects of transport methods that are most sensitive for prediction. The experiments discussed here have shown the importance of accurate stopping power calculations, of an accurate knowledge of the inclusive fragmentation cross sections, including those for isotopes (since the isotopic composition of the fragments affects the estimated ranges and geometrical corrections), of an understanding of higher order generations of secondaries. Experiments, in turn, need to provide information on angular distributions over solid angles comparable with the fragmentation emission angles in order to minimize calculation of detector acceptances. Experimental measurements of light particles, including protons and helium nuclei, and their multiplicities, need to be made in order to account for biologically significant doses at depth. Such data must be systematized in ways accessible to calculation, so that it can be taken into account properly for predictions.

The differences between experimental results for neon and theoretical predictions are of the order of 30-50%, depending on the criterion of comparison. This is surprisingly good and probably

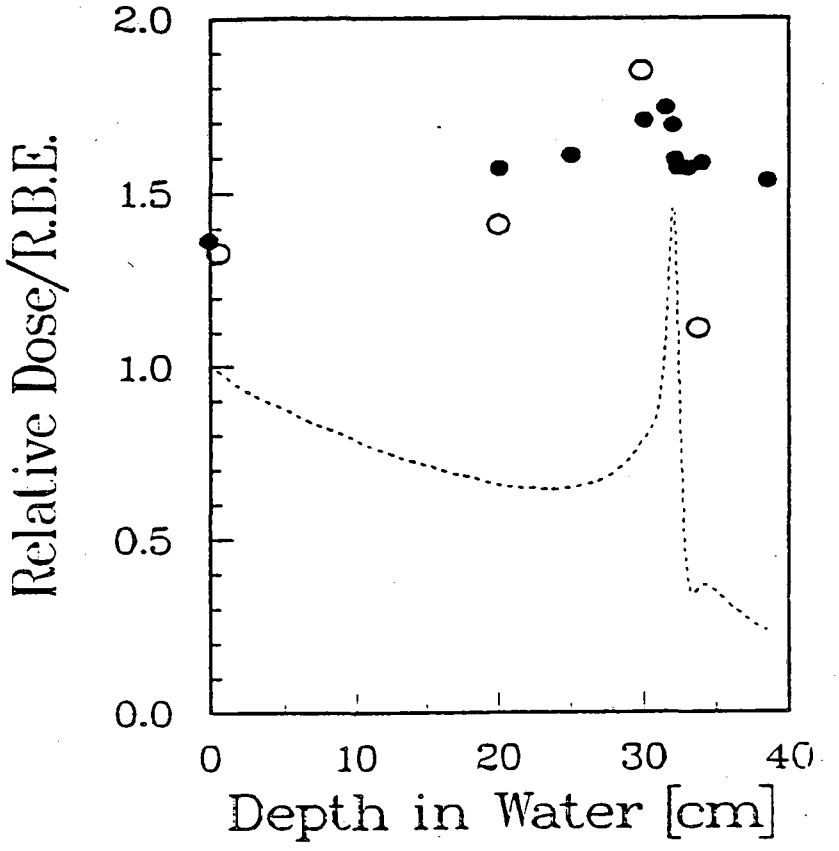

XBL 874-1498

Fig. 9. RBE of mixed radiation field of 670 MeV/u neon.

reflects the extent to which data for neon and lighter particles are available. In the case of iron and the intermediate particles between it and neon there are much fewer data available, both physical and biological. The need for such data is much greater than for neon, since track structure effects, particle multiplicities and other discrepancies from the physics and biology valid for lighter particles can be expected to become much more important.

REFERENCES

1. D. E. Greiner, P. J. Lindstrom, H. H. Heckman, B. Cork, and F. Bieser, Momentum distribution of isotopes produced by fragmentation of relativistic C-12 and O-16 projectiles, *Phys. Rev. Lett.* **35**, 152 (1975).

2. J. P. Wefel, J. M. Kidd, W. Schimmerling, and K. G. Vosburgh, Differential fragmentation cross section for 7.3 GeV nitrogen ions incident on protons, *Phys. Rev.* **C19**, 1380 (1979).

3. E. A. Blakely, F. Q. H. Ngo, S. B. Curtis, and C. A. Tobias, Heavy-ion radiobiology: cellular studies, *Adv. Radiat. Biol.* **11**, 295 (1984)

4. W. Schimmerling, E. L. Alpen, P. Powers–Risius, M. Wong, R.J. DeGuzman and M. Rapkin, The relative biological effectiveness of 670 MeV/A neon as a function of depth in water for a tissue model, *Radiat. Res.* **112**, 436 (1987).

5. R. Silberberg, R. and C. H. Tsao, Partial cross sections in high energy nuclear reactions and astrophysical applications, *Astrophys. J. Suppl.* **25**, 315 (1973).

6. L.W. Townsend and J.W. Wilson, Nuclear cross sections for estimating secondary radiations produced in spacecraft, in: *High-Energy Radiation Background in Space,* eds. A. C. Rester, Jr. and J. I. Trombka, American Institute of Physics, New York 1989, pp.177-191.

7. W. Schimmerling, J. Miller, M. Wong, M. Rapkin, J. Howard, H.G. Spieler, and B. V. Jarret, The fragmentation of 670A MeV Neon-20 as a function of depth in water. I. Experiment, *Radiat. Res.* **120**, 36 (1989).

8. M. R. Shavers, S.B. Curtis, J. Miller and W. Schimmerling, The fragmentation of 670A MeV Neon-20 as a function of depth in water. II. One-generation transport theory, *Radiat. Res.*, in press (1990).

9. S. B. Curtis, Calculated LET distributions of heavy ion beams, *Int. J. Radiat. Oncol. Biol. Phys.* **3**, 87 (1977).

10. W. Schimmerling, S. B. Curtis, and K. G. Vosburgh, Velocity spectrometry of 3.5 GeV nitrogen ions, *Radiat. Res.* **72**, 1 (1977).

11. W. Schimmerling, M. Rapkin, M. Wong, and J. Howard, The propagation of relativistic heavy ions in multielement beam lines, *Med. Phys.* **13**, 217 (1986).

12. H. Bichsel, Charged-particle interactions, in: *Radiation Dosimetry* 2nd ed. Vol. I. Fundamentals, eds. Frank H. Attix and William C. Roesch, Academic Press, Inc., New York 1968, pp. 157-228.

13. J. R. Letaw, Proton production cross sections in proton-nucleus collisions, *Phys. Rev.* **C28**, 2178 (1983).

14. G. D. Westfall, L. W. Wilson, P. J. Lindstrom, H.J. Crawford, D.E. Greiner and H.H. Heckman, Fragmentation of relativistic ^{56}Fe, *Phys. Rev.* **C19**, 1309 (1979).

15. J. W. Wilson, Heavy ion transport in the straight-ahead approximation, NASA TP-2178, (1983).

16. S. B. Curtis, this issue.

LAWRENCE BERKELEY LABORATORY
UNIVERSITY OF CALIFORNIA
INFORMATION RESOURCES DEPARTMENT
BERKELEY, CALIFORNIA 94720